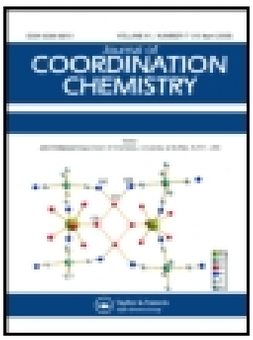

Journal of Coordination Chemistry

ISSN: 0095-8972 (Print) 1029-0389 (Online) Journal homepage: http://www.tandfonline.com/loi/gcoo20

Copper(II) and cobalt(II) complexes of 5-methyl pyrazole-3-carboxylic acid: Synthesis, X−ray crystallography, thermal analysis and *in vitro* antimicrobial activity

Ananyakumari Santra, Paula Brandao, Harekrishna Jana, Gopinath Mondal, Pradip Bera, Abhimanyu Jana & Pulakesh Bera

To cite this article: Ananyakumari Santra, Paula Brandao, Harekrishna Jana, Gopinath Mondal, Pradip Bera, Abhimanyu Jana & Pulakesh Bera (2018): Copper(II) and cobalt(II) complexes of 5-methyl pyrazole-3-carboxylic acid: Synthesis, X−ray crystallography, thermal analysis and *in vitro* antimicrobial activity, Journal of Coordination Chemistry, DOI: 10.1080/00958972.2018.1520984

To link to this article: https://doi.org/10.1080/00958972.2018.1520984

Copper(II) and cobalt(II) complexes of 5-methyl pyrazole-3-carboxylic acid: Synthesis, X−ray crystallography, thermal analysis and *in vitro* antimicrobial activity

ANANYAKUMARI SANTRA†, PAULA BRANDAO‡, HAREKRISHNA JANA¶, GOPINATH MONDAL†, PRADIP BERA†, ABHIMANYU JANA† and PULAKESH BERA1†

†Post Graduate Department of Chemistry, Panskura Banamali College (Vidyasagar University), Panskura R.S, Midnapore (East), West Bengal, India – 721152
‡Department of Chemistry, CICECO, University of Aveiro, 3810−193 Aveiro, Portugal
¶Department of Microbiology, Panskura Banamali College, Panskura R.S, Midnapore (East), West Bengal, India – 721152

The coordination behavior of 5-methylpyrazole-3-carboxylic acid (Hmpca) has been demonstrated by the solid state isolation and characterization of $[Cu(mpca)_2(H_2O)]\cdot 3H_2O$ (**1**) $[Cu(mpca)_2]\cdot H_2O$ (**2**) and $[Co(mpca)_2(H_2O)_2]$ (**3**). The new compounds are characterized by X-ray crystallography, thermogravimetric analysis and DFT study. The redox properties of the complexes are examined by cyclic voltammetric analysis. The antibacterial and antifungal activities of the compounds against eight bacteria (*E. coli*, *S. fecalis*, *B. subtilis*, *K. pneumonia*, *P. vulgaris*, *S. aureus*, *P. aeruginosa* and *S. typhi*) and two fungi (*A. flavus* and *C. albicans*) are screened using modified agar well diffusion method. The metal complexes demonstrate better inhibition on all bacteria and fungi than the ligand. The high lipophilicity of the complexes accounts for good inhibitory action toward microbes. Among the reported complexes, **3** emerges as an excellent antifungal agent and a better antibiotic than standard fluconazole. The structure and activity relationship indicates that complexes having sufficient Jahn-Teller distortion with high *logP* values, cross the cell membrane of the microbes creating intercellular damage.

Keywords: Pyrazolyl; Inner-metallic; Thermogravimetry; Antibacterial-antifungal; Mono/polymeric

1. Introduction

Heterocyclic compounds containing nitrogen, sulfur and oxygen and their metal complexes are biologically active materials towards bacteria, fungi and viruses [1-5]. Heterocyclic compounds

1Corresponding author. Email: pbera.pbc.chem@gmail.com

containing pyrazole rings have interest due to their applications in the pharmaceutical and agrochemical industries [6]. Pyrazole derivatives have wide range of applications like anti-hyperglycemic [7], analgesic [8], anti-inflammatory [9], antipyretic [10], antibacterial [11], hypoglycaemic [12] and sedative−hypnotic activities [13]. Pyrazole derivatives such as celecoxib, rimonabant, fomepizole and sildenafil were established as selective drugs [14]. Celecoxib demonstrated anti-inflammatory effect and inhibited cox-2 [15]. Rimonabant is a cannabixiod receptor and is used for obesity treatment. Fomepizole and bindenafil inhibit alcohol dehydrogenase and phosphodiesterase, respectively [16]. Some pyrazole derivatives also have non nucleoside HIV−1 reverse transcriptase inhibitory activities [17-19]. Their transition metal complexes are also active metallobiomolecules. The acid and amido derivatives of pyrazole compounds are important heterocycles for synthesis of metallobiomolecules [20]. Copper and cobalt complexes of pyrazolyl derivatives showed excellent antibacterial and antifungal activities for generation of several coordination and non−covalent interactions [20-23]. For these reasons, large numbers of copper complexes were synthesized to screen the biological activities and some of them were active both *in vivo* and *in vitro* [15, 23]. Fascinated by the significant biological applications of transition metal complexes of pyrazolyl compounds, comprehensive work has been taken up to synthesize and screen the antimicrobial activity of pyrazole derivatives. Herein we report the synthesis, characterization and antimicrobial activities of three new complexes of copper(II) and cobalt(II) derived from 5–methylpyrazole–3–carboxylic acid. The structure-activity relationship has been discussed.

2. Experimental

2.1. *Materials*

Reagent grade $CuCl_2{\cdot}2H_2O$ and $Co(NO_3)_2{\cdot}6H_2O$ were purchased from Merck India Chemical Company and used without purification. The salt $Cu(ClO_4)_2{\cdot}6H_2O$ was prepared by laboratory process from $CuCO_3$ (Merck, India) and perchloric acid (Merck, India). Solvent ethanol (Changshu Yangyuan Chemical, China), methanol (Merck, India) and dichloromethane (Merck, India) were dried and distilled before use. 1-Octanol, hydrazine hydrate, ethyl acetate, pyruvic acid and hydrazine sulphate were purchased from Himedia, India. *Caution!* Perchlorate salts are explosive. Care should be taken in handling the perchlorate salts.

2.2. *Characterization*

Elemental analyses (C, H, N, and S) of the ligand and complexes were performed using a FISONS EA−1108 CHN analyzer. The molar conductance of 10^{-3} (M) solutions of **1**, **2** and **3** in DMF:MeOH (1:1) were measured at 30 °C using a Thermo Orion model 550A conductivity meter and a dip-type cell with platinized electrode. The FTIR analyses were performed by using a Perkin Elmer Spectrum Two Spectrophotometer (400–4000 cm^{-1}). The samples were prepared as KBr pellets using anhydrous KBr salt. The magnetic susceptibility measurements were done using a Sherwood Scientific Cambridge (UK) magnetometer. UV–Visible absorption spectra of samples were recorded on a Perkin Elmer Lambda 35 spectrophotometer from 200–800 nm at room temperature. Single crystal X–ray diffractions (XRD) of **1-3** were carried out on a Bruker SMART APEX II X–ray diffractometer equipped with graphite–monochromatic Mo−Kα radiation (λ = 0.71073 Å) and 16 CCD area detector. The intensity data were collected in the π and ω scan mode, operating at 50 kV, 30 mA at 296 K [24]. The data reductions were performed using SAINT and SADABS programs [25]. All calculations in the structural solution and refinement were performed using the Bruker SHELXTL program [26]. The structures were solved by the heavy atom method and refined by full-matrix least-squares methods. All non–hydrogen atoms were refined anisotropically; hydrogens were geometrically positioned and fixed with isotropic thermal parameters. The final electron density maps showed no significant difference. Cyclic voltammetry studies were performed at room temperature in methanol using tetrabutylammonium perchlorate as a supporting electrolyte on a CH Instrument electrochemical workstation model no. CHI630E. The conventional three-electrode assembly is comprised of a platinum working electrode, a platinum wire auxiliary electrode and a Ag/AgCl reference electrode. Thermogravimetric analysis was performed using a Perkin Elmer Thermal Analyzer TGA4000 instrument at a heating rate 20 °C/min under nitrogen.

2.3. *Synthesis of ligand and metal complexes*

2.3.1. Synthesis of 5–methylpyrazole–3–carboxylic acid (Hmpca). 5–Methylpyrazole–3–carboxylic acid (Hmpca) was prepared from the hydrolysis of 5–methylpyrazole–3–carbohydrazide (mpch) [27]. Aqueous solution of sodium ethyl acetopyruvate (A) (10 g, 0.05 mol) is taken in a 250 mL round bottom flask and allowed to react with hydrazine sulphate (7 g, 0.05 mol) in the presence of anhydrous Na_2CO_3 (scheme 1). A light yellow product ethyl 5–

methylpyrazole–3–carboxylate (B) is obtained. The ester (B) separated from the solution is filtered off, washed with water and dried in an oven at 100 °C. Recrystallization from aqueous ethanol gave the pure ester (B) in colorless form melting at 82 °C. The dried ester (0.04 mol, 6.2 g) is allowed to reflux with hydrazine hydrate (100%) (0.06 mol, 3.0 g) at water bath temperature for 1 h. A white crystalline precipitate of 5–methylpyrazole–3–carbohydrazide (mpch) is obtained which is filtered off, washed with aqueous ethanol and dried in a vacuum desiccator. The dried mpch melts at 153 °C. The yield is 4.2 g (75%). The dry mpch (15 mmol, 2.1 g) is taken in excess hydrazine hydrate (30 mL) and refluxed for 5 h. The desired ligand (Hmpca) is obtained by removing excess hydrazine by vacuum distillation. The product thus obtained is recrystallized from dry ethanol. Purity of the product was checked by the determination of melting point (M.P. 239 °C).

2.3.2. Synthesis of $[Cu(mpca)_2(H_2O)]\cdot 3H_2O$ (1) and $[Cu(mpca)_2]\cdot H_2O$ (2). Hmpca (5 mmol, 0.63 g) dissolved in 15 mL in dry methanol is allowed to mix with a methanolic solution of $CuCl_2\cdot 2H_2O$ (2.25 mmol, 0.38 g) (20 mL) in a 100 mL round bottom flask. The resulting blue solution is refluxed for 6 h whereupon a blue crystalline product separates. The product is filtered off, washed with methanol and dried over silica gel. The yield is 0.86 (72%) for $[Cu(mpca)_2(H_2O)]\cdot 3H_2O$ (**1**). Elemental analysis for **1** ($C_{10}H_{14}CuN_4O_6$): Calculated: C, 31.10; H, 4.66; N, 14.53 and Found: C, 31.05; H, 4.54; N, 14.85. IR assignments (in cm^{-1}): $\nu_{(C=N)}$ (1425), $\nu_{(C-N)}$ (1299), $\nu_{(N-N)}$ (1041) and $\nu_{(C-O)}$ (1627).

In similar way, $Cu(ClO_4)_2\cdot 6H_2O$ (2.25 mmol, 0.83 g) in 20 mL dry methanol is mixed with a dry methanolic solution (15 mL) of Hmpca (5 mmol, 0.63 g). The resulting solution is refluxed for 4 h; slow evaporation of the solution at room temperature furnished blue crystalline compound which is filtered off, washed with methanol and dried over silica gel. The yield is 0.51 g (68%) for $[Cu(mpca)_2]\cdot H_2O$ (**2**). Elemental analysis for **2** (when n=1) ($C_{10}H_{12}CuN_4O_5$): Calculated: C, 36.16; H, 3.61; N, 16.87 and Found: C, 36.29; H, 3.42; N, 16.91. IR assignments (in cm^{-1}): $\nu_{(C=N)}$ (1369), $\nu_{(C-N)}$ (1285), $\nu_{(N-N)}$ (1034) and $\nu_{(C-O)}$ (1550).

2.3.3. Synthesis of $[Co(mpca)_2(H_2O)_2]$ (3). Hmpca (5 mmol, 0.63 g) dissolved in 15 mL hydrazine hydrate (100%) is mixed with a hot methanolic solution of $Co(NO_3)_2\cdot 6H_2O$ (20 mL) (2.25 mmol, 0.65 g) with constant stirring. The resulting solution is refluxed for 4 h and the solid

thus obtained is filtered, washed with dry methanol, and dried in vacuum. Yield is 0.54 g (71%) for $C_{10}H_{14}CoN_4O_6$ (**3**). Elemental analysis: Calculated: C, 34.76; H, 4.05; N, 16.22 and Found: C, 34.56; H, 3.89; N, 16.57. IR assignments (in cm^{-1}): $\nu_{(C=N)}$ (1476), $\nu_{(C-N)}$ (1271), $\nu_{(N-N)}$ (1041) and $\nu_{(C-O)}$ (1697).

Complexes **1**, **2** and **3** are soluble in common polar solvents like methanol, ethanol, DMF, and DMSO. The molar conductivity values of 20, 15 and 23 $\Omega^{-1}cm^2mol^{-1}$ for **1**, **2** and **3**, respectively, in DMF:MeOH (1:1) with concentration 10^{-3} (M) are indicative of nonelectrolyte nature of the complexes. The observed spin only magnetic moment values are 2.32, 2.22 and 3.58 BM for **1**, **2** and **3**, respectively. The magnetic moment measurements indicate high spin cobalt(II) center in **3**.

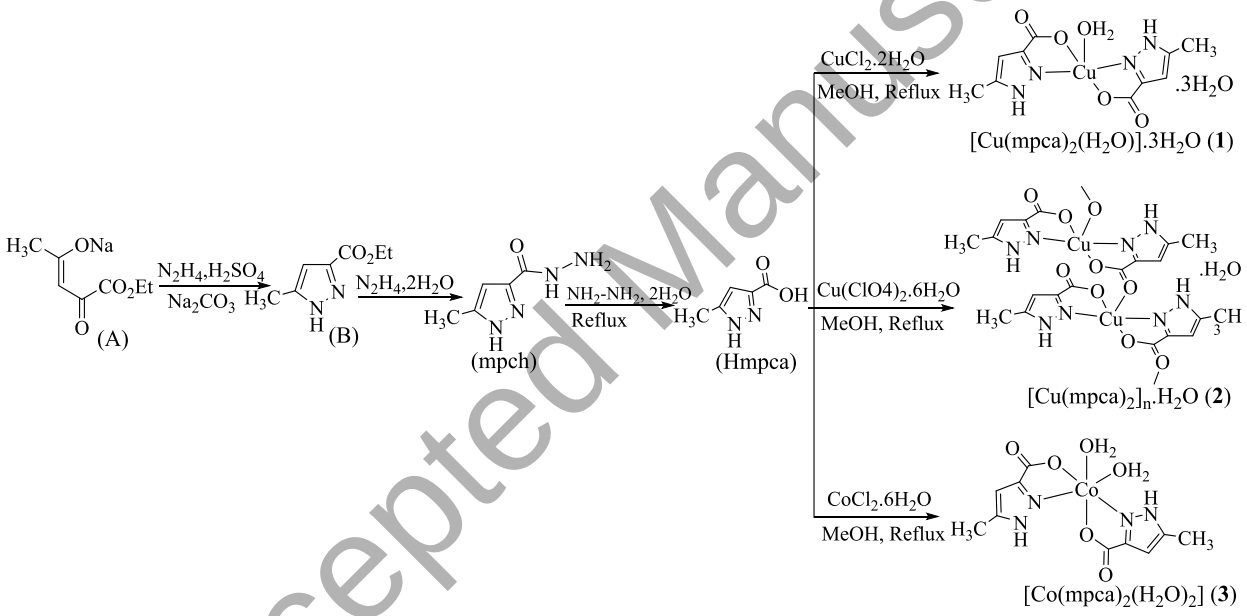

Scheme 1. Synthesis of Hmpca ligand and **1-3**.

2.4. *Determination of the logP by using the shake−flask method*

Lipophilicity of the ligands and complexes are determined by calculating *logP* values according to the shake-flask method [6]. Compounds under investigation are weighted out accurately and partitioned between equal volumes of water and 1-octanol (5 mL each) by shaking for 30 h at room temperature to assure full partitioning of the analyzed compounds between water and 1-octanol phases. Then, the solution is centrifuged at 3500 rpm for 10 minutes to separate into two layers. The concentration of the compounds in different layers is estimated by the optical

density values obtained from UV-Vis spectroscopy. Concentration of organic, aqueous phase and log*P* values are in table 1.

2.5. *DFT calculations*

The ground state electronic structure calculations have been carried out using the X-ray coordinates of the complex with the help of DFT [28] methods with the Orca 2.7 program [29]. Becke's hybrid function [29] with the Lee–Yang–Parr (LYP) correlation function [30] was used throughout the study. LANL2DZ valence and effective core potential functions were used. All energy calculations were performed using the self-consistent field "tight" option of the Orca 2.7 program to ensure sufficiently well converged values for the state energies.

2.6. *Determination of antibacterial and antifungal activity*

Antibacterial sensitivity is tested by the agar well diffusion method using Mueller–Hilton agar media. The said diffusion method is employed for the determination of antibacterial activities of the compounds following the method described by Vanden Berghe and Vlietinck in 1991 [31]. The compounds are dissolved with required amount of methanol to make up a concentration 5000 μg/mL. From this stock solution different concentrations of working solution (ranges from 1000 to 25 μg/mL) was prepared. Eight species of pathogenic bacteria, *Escherichia coli*, *Salmonella typhi*, *Klebsiella pneumoniae*, *Staphylococcus aureus*, *Proteus vulgaris*, *Pseudomonas aeruginosa*, *Bacillus subtilis* and *Streptococcus faecalis*, are used to screen the antibacterial activities of the compounds [32]. Pathogenic bacterial strains are incubated at 37 °C for 24 h in sterile nutrient broth. The inocula size of swabbed pathogen was adjusted to deliver 10^6 CFU/mL on the surface of Mueller−Hilton agar media. 25 mL of Mueller–Hinton Agar media and 100 μL inoculums of bacterial strain are allowed to solidify in petridishes. Wells are made into solidified agar media with the help of sterilized cup−borer. 100 μL of prepared sample solution is poured into the respective wells and the plates are incubated overnight at 37 °C. Methanol is used as a control. The experiment is repeated three times under strict aseptic condition and the antibacterial activity of each compound was expressed in terms of the mean diameter of zone of inhibition (in cm) produced by the respective compound.

Similarly, antifungal sensitivity is tested by the agar well diffusion method using PD agar media [32]. Two species of pathogenic fungi, *Aspergillus flavus* and *Candida albicans*, are used

to screen the antifungal activity of the pyrazolyl compounds. Pathogenic fungal strain are inoculated in sterile potato dextrose broth and incubated at 25 °C for 48 to 72 h. Petri dishes containing 25 mL of potato dextrose agar with 100 μL inoculums of fungal strain and media is allowed to solidify. The remaining work up process is similar to that of antibacterial sensitivity test. The stock solution (5000 μg/mL) was made by dissolving the antibiotic in sterile distilled water. From this stock solution 1000 μg/mL was prepared for the determination of the sensitivity of fungi.

3. Results and discussion

Hydrolysis of 5–methyl pyrazole–3–carbohydrazide (Hmpch) occurs in the presence of hydrazine hydrate. The title complexes are obtained by reaction of the ligand with the corresponding metal salt. The alkaline hydrolysis of mpch gives high yield of the ligand in the present procedure. The anion in the solution influences the crystallization as evidenced by the formation of different copper(II) complexes. Monomeric and polymeric copper(II) complexes are isolated in the presence of chloride and perchlorate ions, respectively. This is an instance of anion dependent crystallization of copper(II) complexes. On the other hand, cobalt(II) salt in the solution always furnish monomeric complex of Hmpca irrespective of the anion present in the reaction medium. The reducing environment prevents the oxidation of cobalt(II) species during reaction. The use of hydrazine as solvent has the advantage to prepare complexes of cobalt(II). The spin only magnetic moment values of the complexes reveal the presence of one and three unpaired electrons in copper(II) and cobalt(II) complexes.

3.1. *FTIR analysis*

The important IR assignments (in cm^{-1}) of the complexes are shown in figure 1. The stretching frequencies of the C=N, C−N and N−N(pyrazole) bonds are obtained in the range 1425-1467, 1271-1299 and 1034-1041 cm^{-1}, respectively, in the complexes. Similar IR frequencies are also observed in several pyrazole derivatives [33]. All peaks are obtained in lower frequency range in **2** than those observed in **1** and **3**. This proves the polymeric nature of **2** where polymerization effectively reduced the respective bond orders. The peak at 1550-1697 cm^{-1} in the complexes can be assigned for the stretching vibration of C−O of carboxylate. The observed lower

frequency range of ν(CO) in the complexes with respect to free carboxylic acid (1690-1710 cm^{-1}) revealed that the coordination occurred through oxygen of the acid group [33, 34].

3.2. *Single crystal X-ray crystallography*

Single crystal X-ray analyses of the complexes provide the molecular arrangement and coordination environment of the transition metal chelates. Figure 2 shows the ORTEP diagram of **1** and crystal refinement parameters are given in table 2. Selected bond lengths and angles of the complexes are given in tables 3 and 4, respectively. The 5–methylpyrazole–3–carboxylic acid (Hmpca) acts as a uninegative bidentate ligand, coordinating through N and O. Complex **1** is a monomer and crystallizes with space group Pī. The role of water molecules in the crystal packing of **1** is very important. The 1D propagation of molecule competes with the parallel propagation of molecules of water of crystallization making a cylindrical channel of water. The D…A bond distance (2.03 Å) indicates considerable H−bonding in the molecule. The H bonds are shown in figure S1 and the corresponding values are given in table S1. Copper is square pyramidal with the base formed by two nitrogen and two oxygen atoms of $mpca^-$. The fifth coordination site is occupied by a water molecule (figure 2). Copper(II) is coordinated by pyrazolyl N and anionic O of the acid group of $mpca^-$. The bond lengths Cu−N1 and Cu−N2 are 1.941 Å and 1.954 Å, respectively, and the bond lengths Cu−O2 and Cu−O4 are equal (1.963 Å), whereas the Cu–O1 length is 2.466 Å, which indicates the axial position of the square pyramidal structure is occupied by H_2O (table 3).

The same ligand furnishes a polymeric copper(II) complex in the presence of $Cu(ClO_4)_2 \cdot 6H_2O$ designated as **2**. Figure 3 represents the ORTEP diagram of **2**, where the copper ion completed five coordination sites to form a distorted square pyramidal complex with the pyrazolyl N and carboxylic O of $mpca^-$. Four basal positions are occupied by N and O atoms of two $mpca^-$ and the fifth position is occupied by the oxygen of the $mpca^-$ of a neighboring molecule. A polymeric structure is formed through Cu–O–Cu bonding (figure 4). The propagation of polymeric chains in the structure is facilitated by several non-covalent interactions. The π-π interactions were found with centroid to centroid distance 3.739 Å in **1** (figure S2). Contribution of CH-π interaction is also interpreted with centroid to HC 3.15 Å. The H-bond interactions of **2** are shown in figure S3.

In **3**, the cobalt is octahedrally surrounded by the ligand as shown in figure 5. The asymmetric unit contains half of the whole molecule where a C2 axis passes through cobalt and symmetric operation C2 generates the whole molecule. The *cis* form is predominant in the solid state. This may be due to the process of crystallization of the compound in the polar solvent [35]. The typical higher values of Co−N(pz) and Co−O(carboxylate) than reported Co^{III}–N and Co^{III}–O bonds in octahedral complexes clearly suggest +2 oxidation state of cobalt in **3** [35]. In the structure of **3**, the H-bonding aspects are very important. Strong H-bonding occurs in each H attached with pyrazole N and coordinated water with oxygen. H-bonds are extended three dimensionally as shown in figure S4. No CH-π interaction was involved in the proposed structure. Ligand containing N–N donor sites are involved for coordination and two water molecules are attached to the cobalt making it six-coordinate octahedral (figure 5). The cobalt(II) octahedral complex is stabilized by strong chelation through the donor pyrazolyl nitrogen and carboxylate oxygen.

3.3. *Thermogravimetric analysis*

Thermal decomposition of all three complexes is carried out. As shown in figure 6, TG curve of **1** shows three significant mass losses at 100-135 °C (18.3%), 135-350 °C (5.6%) and 340-700 °C (47.1%). The first step corresponds to the loss of three moles of water of crystallization followed by the second step which accounts for the loss of one mole of coordinated water from the coordination site. About 47.1% mass loss in the third stage of decomposition may be loss of two moles of methyl pyrazole. There is similarity in the decomposition of **2** with the isostructural **1** but the decomposition steps are not clearly observed in **2**. The reason may be the polymeric nature of **2**. Unlike **1**, the decomposition of **2** starts at RT which reveals that the sample may contain moisture. A mass loss up to 300 °C is about 18% (*calc.* 18.68%) which may be the combined loss of one unit CO_2 and one mole of water of crystallization. The certain mass losses at 290-390 °C is the loss of remaining organics *i.e.*, methyl pyrazole unit giving CuO residue (23.96%). Further heating of the compound beyond 500 °C metallic copper is obtained with residual percentage 19.1 [36]. As shown in figure 6 (c), the decomposition of **3** starts at 150 °C giving a weight loss about 86%, which can be attributed to the combined lose of two moles of coordinated water molecules (calc. 10.42%) preceding the loss of two moles of 5-methyl pyrazole-3-carboxylic acid (calc. 71.84%) giving a residue 17% of metallic cobalt [33, 37].

3.4. *Cyclovoltammetry study*

The electrochemical behaviors of the present compounds have been studied as these categories of compounds have wide applications in biology and chemistry. The redox properties give insight into their metabolic facts and biological activities. Copper(II) complexes **1** and **2** in methanol solution (10^{-3} M) in the presence of tertiary butyl ammonium perchlorate as a reference electrolyte versus Ag/AgCl, saturated KCl, at a scan rate 100 mVs^{-1}, display irreversible reductive responses at −0.561V (C_1) in **1** and −0.346V (C_1) in **2** which correspond to the reduction Cu(II)→Cu(I) as shown in figure 7. The other peak on cathodic scan at +0.559V (C_2) in **1** and +0.738V (C_2) in **2** can be assigned for the reduction of Cu(I) to Cu(0). In the subsequent anodic scan, the anodic counterparts (A1, A2) are not prominent. A broad peak at +0.979V (A_2) in **1** and +1.153V (A_2) in **2** are assigned for Cu(0)→Cu(I). The difference in the values of reduction potential in the copper complexes may be due to the different coordination environment around copper(II) *e.g.*, monomeric structure of **1** and polymeric structure of **2**, respectively [38]. The CV of **3** also shows irreversible redox process. Irreversible reductive responses at −0.253V (C_1) and +0.262V (C_2) correspond to Co(III)→Co(II) and Co(II)→Co(I), respectively. The only one observable anodic peak at +0.458 (A_2) can be attributed to the oxidation of Co(II)→Co(III).

3.5. *DFT study*

Density functional theory is used to give insight about the structural aspects of the prepared complexes. Representative complexes **1** and **3** are investigated by DFT study. DFT study of **1** shows that HOMO is completely localized on carboxylic acid group of the ligand molecule; similar features are also observed for HOMO(n-1) and LUMO(n+1). However, LUMO in **1** is mainly localized both on pyrazole ring and carboxylic acid group (figure 8). Coordinated water molecule does not contribute much to the HOMO(n-1), HOMO, LUMO and LUMO(n-1). In **3**, HOMO(n-1) and HOMO are fully localized on carboxylic acid group and coordinated water molecules. Pyrazole moiety does not contribute to the HOMO(n-1) and HOMO. LUMO and LUMO(n+1) of **3** are mainly composed with pyrazole unit, carboxylic acid group and coordinated water molecules. The theoretical studies register that the coordinated water

molecules in **3** have higher involvement with the metal center than **1**. Thus it can be concluded that **1** is more labile than **3** with respect to water substitution.

3.6. *Antimicrobial activity*

The diploid nature and longer generation time of fungi compared to bacteria make them different with respect to interaction with antimicrobial agents [39-41]. Most of the antibacterial agents inhibit the formation of peptidoglycan of cell wall resulting in cell death. Other prominent ways to destroy bacteria are protein synthesis inhibitors, topoisomerase inhibitor and metabolic pathway inhibitor. Whereas most antifungal agents target the formation and function of ergosterol which is an important component of fungal cell membrane. The ability of the ligands and complexes to inhibit the growth of several bacteria and fungi are assessed using disc diffusion, agar well diffusion, and minimum inhibitory assays. The *in vitro* antimicrobial activities are given in table 5 and MIC values of the compounds are presented in table 6. Camera views of the agar experiments are provided in the Supplementary Data (figure S5). Results show that the antimicrobial activities of the complexes are greater than the ancillary ligands *i.e.*, Hmpca and mpch. This can be explained on the basis of lipophilic character of the compounds. The lipophilicity of a compound is the measure of cell membrane permeation. Mostly disposition ability of a drug depends on the capacity to cross the cell membrane [42, 43]. The general trend of the logP (where P is the partition coefficient) values is 0.645 (**3**) > 0.396 (**1**) > 0.253 (Hmpca) > 0.174 (mpch) > 0.101 (**2**) (table 1). The antibacterial effect of the tested compounds follows the above logP order. Complex **3** has the highest logP (0.645) and exhibits the highest antimicrobial property. The lowest logP value is attesting the lowest activity of **2**. The polymeric nature of **2** restricts the distribution of molecule in the organic (1-octanol) phase compared to monomeric complexes **1** and **3**. The *logP* order among the ligands can be explained considering the increased polarity of the ligands. 5-Methyl pyrazole carbohydrazide (mpch) and/or 5-methyl pyrazole 3-carboxylic acid (Hmpca) is expected to have higher polarity than the metal complexes. Both the ligands, mpch and Hmpca, which differ from each other solely by their functional group, exhibit low antibacterial activity (MIC values 500−600 μg/mL) against *K. pneumonia* and *C. albicans* compared to metal complexes. The complexes obtained from the reaction of ligand and metal ions are where the primary charge(s) of the metal ion is satisfied by the ligand molecule. Absence of any free anion(s) in the complexes makes them lipophilic in

nature. Lipophilicity of compound favors permeation through the lipid layer of the cell membrane. The present study concludes that complexes with high *logP* show better antimicrobial activity than the original chelator. Among the complexes, cobalt(II) complex (**3**) exhibits the greatest antimicrobial activity with MIC values 25−100 μg/mL and the lowest activity is exhibited by polymeric **2** against different bacteria and fungi. These findings are graphically represented in figure 9.

3.7. *Structure-activity relationship*

Sensitivity study and the MIC values reveal that **1** and **3** show best results (figure 7). Copper(II) (d^9) and high spin cobalt(II) (d^7) have electron arrangement $(d_{z^2})^2(d_{x^2-y^2})^1$ and $(d_{z^2})^1$, respectively. The asymmetric arrangement registers a strong tetragonal distortion which allows weak coordination with H_2O in the axial position. The distortion in **1** and **3** makes them labile with respect to H_2O substitution. DFT results also suggest higher lability of the water molecule in **1** than **3**. The lability of the complexes favors oxygen binding to the metal center, which further leads to generation of different reactive oxygen species (ROS). The generated ROS are responsible for microbial cell destruction. The lesser activity of **2** than **1** and **3** can be explained on the basis of non availability of coordinated water molecule in the coordination site and polymeric structure making it inert with respect to ligand substitution. Additionally, the compounds have high value of lipophilicity (log*P*) (*P* refers partition coefficient) (table 1). The high lipophilicity shows high permeation to the cell wall of the microbes inhibiting metabolism and protein synthesis.

4. Conclusion

Complexes of copper(II) and cobalt(II) with 5-methylpyrazole–3–carboxylic acid (Hmpca) are synthesized and characterized by X-ray crystallography, TGA, DFT and cyclic voltammetry study. Both monomeric and polymeric copper(II) complexes are obtained from the influence of different counter ions in the reaction mixture. Monomeric **1** adopts a square pyramidal structure where pyrazolyl N and O (carboxylate) of ligand occupy the corners of the square plane, and the axial position is occupied by a water molecule. The polymeric structure of **2** is obtained where the square planes are attached with other square planes through an axial O (carboxylate). Cobalt(II) complex (**3**) has distortion in its structure due to Jahn-Teller effect which holds two

water molecules weakly. The loosely bound water molecules are labile with respect to ligand substitution. The lability of the present complexes favors formation of reactive oxygen species (ROS) for the cell destruction of microbes under investigation. Moreover, the present complexes have high lipophilicity showing better permeation to the cell wall leading to cell death. These combining effects of lability and lipophilicity need to be explored to search for new drugs.

Supplementary data

CCDC 1826509, 1826510 and 1826511 for **1**, **2** and **3**, respectively. Crystallographic data can be obtained free of charge on application to CCDC, 12 Union Road, Cambridge CB2 1EZ, UK; Fax: (+44) 1223 336033; E-mail: deposit@ccdc.cam.ac.uk.

Acknowledgement

We gratefully acknowledge the grant from Council for Scientific and Industrial Research (CSIR), Government of India through the project [No. 1(2858)/16/EMR−II]. Panskura Banamali College acknowledges the grants received from Department of Science and Technology (DST), Govt. of India through FIST program (Sanction no. SR/FST/College−295 dated 18/11/2015).

Conflict of interest

The authors declare no conflict of interest.

References

[1] M.K. Kathiravan, A.B. Salake, A.S. Chothe, P.B. Dudhe, R.P. Watode, M.S. Mukta, S. Gadhwe. *Bioorg. Med. Chem.*, **20**, 5678 (2012).

[2] Y. Bansal, O. Silakari. *Bioorg. Med. Chem.*, **20**, 6208 (2012).

[3] H. Goker, C. Kus, D.W. Boykin, S. Yildiz, N. Altanlar. *Bioorg. Med. Chem.*, **10**, 2589 (2002).

[4] M. Boiani, M. Gonzalez. *Mini Rev. Med. Chem.*, **5**, 409 (2005).

[5] O.O. Guven, T. Erdogan, H. Goker, S. Yildiz. *Bioorg. Med. Chem. Lett.*, **17**, 2233 (2007).

[6] B. Kupcewicz, M. Ciolkowski, B.T. Karwowski, M. Rozalski, U. Krajewska, I.P. Lorenz, P. Mayer, E. Budzisz. *J. Mol. Struct.*, **1052**, 32 (2013).

[7] R. Kenchappa, Y.D. Bodke, A. Chandrashekar, M. ArunaSindhe, S.K. Peethambar. *Arabian J. Chem.*, **10**, S3895 (2017).

[8] A. Almasirad, M. Tajik, D. Bakhtiari, A. Shafiee, M. Abdollahi, M.J. Zamani, R. Khorasani, H. Esmaily. *J. Pharmacy Pharmaceutical Sci.*, **8**, 419 (2005).

[9] O. Rosati, M. Curini, M.C. Marcotullio, A. Macchiarulo, M. Perfumi, L. Mattioli, F. Rismondo, G. Cravotto. *Bioorg. Med. Chem.*, **15**, 3463 (2007).

[10] A.A.M. Eissa, N.A.H. Farag, G.A.H. Soliman. *Bioorg. Med. Chem.*, **17**, 5059 (2009).

[11] G. Mondal, H. Jana, M. Acharjya, A. Santra, P. Bera, A. Jana, A. Panja, P. Bera. *Med. Chem. Res.*, **26**, 3046 (2017).

[12] P.A. Datar, S.R. Jadhav. *Int. J. Med. Chem.*, **2015**, 10 (2015) vol. 2015, Article ID 670181, 10 pages, 2015. https://doi.org/10.1155/2015/670181.

[13] S.K. Kashaw, V. Gupta, V. Kashaw, P. Mishra, J.P. Stables, N.K. Jain. *Med. Chem. Res.*, **19**, 250 (2010).

[14] A. Ansari, A. Ali, M. Asif, Shamsuzzaman. *New J. Chem.*, **41**, 16 (2017).

[15] M.A.-A. El-Sayed, N.I. Abdel-Aziz, A.A.-M. Abdel-Aziz, A.S. El-Azab, Y.A. Asiri, K.E.H. Eltahir. *Bioorg. Med. Chem.*, **19**, 3416 (2011).

[16] S. Mert, R. Kasimogullari, T. Ica, F. Colak, A. Altun, S. Ok. *Eur. J. Med. Chem.*, **78**, 86 (2014).

[17] K. Senga, T. Novinson, R.H. Springer, R.P. Rao, D.E. O'Brian, R.K. Robins, H.R. Wilson. *J. Med. Chem.*, **18**, 312 (1975).

[18] S.P. Singh, D. Kumar. *Heterocycles*, **31**, 855 (1990).

[19] F. Karcı, N. Şener, M. Yamaç, İ. Şener, A. Demirçalı. *Dyes Pigm.*, **80**, 47 (2009).

[20] M. Sobiesiak, T. Muzioł, M. Rozalski, U. Krajewska, E. Budzisz. *New J. Chem.*, **38**, 5349 (2014).

[21] J. Liu, H. Zhang, C. Chen, H. Deng, T. Lu, L. Ji. *Dalton Trans*, **1**, 114 (2003).

[22] R. Nagane, M. Chikira, M. Oumi, H. Shindo, W.E. Antholine. *J. Inorg. Biochem.*, **78**, 243 (2000).

[23] F. Arjmand, B. Mohani, S. Ahmad. *Eur. J. Med. Chem.*, **40**, 1103 (2005).

[24] Bruker, SAINT (Version 6.28a) and SADABS (Version 2.03) Data reduction and absorption correction program. Bruker AXS Inc, Madison, Wisconsin (2001).

[25] Bruker, SMART (Version 5.625) Data collection program. Bruker AXS Inc., Madison, Wisconsin (2001).

[26] G.M. Sheldrick, SHELXL-97, Crystal Structure Refinement Program, University of Göttingen (1997).

[27] P. Bera, N. Saha, S. Kumar, D. Banerjee, R. Bhattacharya. *Transition Met. Chem.*, **24**, 425 (1999).

[28] A.D. Becke. *J. Chem. Phys.*, **98**, 5648 (1993).

[29] R.G. Parr, W. Yang, *Density Functional Theory of Atoms and Molecules*, Oxford University Press, Oxford (1989).

[30] C. Lee, W. Yang, R.G. Parr. *Phys. Rev. B*, **37**, 785 (1998).

[31] D.A. Vanden Berghe, A.J. Vlietinck, Screening methods for antibacterial and antiviral agents from higher plants. In: Dey PMp, Harbone J B (eds) Methods in plant biochemistry. Academic, London, **47** (1991).

[32] A. Nostro, M.P. Germanò, V. D'Angelo, A. Marino, M.A. Cannatelli. *Lett. Appl. Microbiol.*, **30**, 379 (2000).

[33] K.M. Szecsenyi, V.M. Leovac, V.I. Cesljevic, A. Kovacs, G. Pokol, G. Argay, A. Kalman, G.A. Bogdanovic, Z.K. Jacimovic, A.S. Bireg. *Inorg. Chim. Acta*, **353**, 253 (2003).

[34] P. Bera, S.I. Seok. *J. Solid State Chem.*, **183**, 1872 (2010).

[35] A. Panja, N.C. Jana, A. Bauzá, A. Frontera, C. Mathonière. *Inorg. Chem.*, **55**, 8331 (2016).

[36] P. Bera, S.I. Seok. *Solid State Sci.*, **14**, 1126 (2012).

[37] A.A. Nejo, G.A. Kolawole, A.O. Nejo. *J. Coord. Chem.*, **63**, 4398 (2010).

[38] E. Franco, E. Lopez-Torres, M.A. Mendiola, M.T. Sevilla. *Polyhedron*, **19**, 441 (2000).

[39] J. Joseph, G. B. Janaki, K. Nagashri, R.S. Joseyphus. *J. Coord. Chem.*, **70**, 242 (2017).

[40] S. Bharti, M. Choudhary, B. Mohan. *J. Coord. Chem.*, **71**, 284 (2018).

[41] S.S. Jawoor, S.A. Patil, S.S. Toragalmath. *J. Coord. Chem.*, **71**, 271 (2018).

[42] G. Mondal, H. Jana, M. Acharjya, A. Santra, P. Bera, A. Jana, A. Panja, P. Bera. *Med. Chem. Res.*, **26,** 3046 (2017).

[43] E. Budzisz, I.-P. Lorenz, P. Mayer, P. Paneth, L. Szatkowski, U. Krajewska, M. Rozalski, M. Miernicka. *New J. Chem.*, **32**, 2238 (2008).

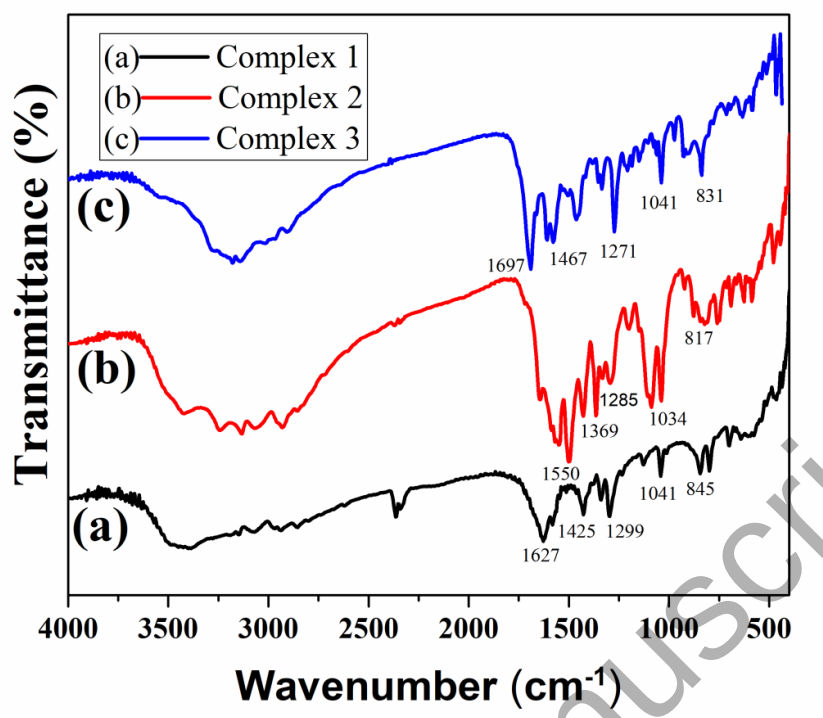

Figure 1. FTIR analysis of **1-3**.

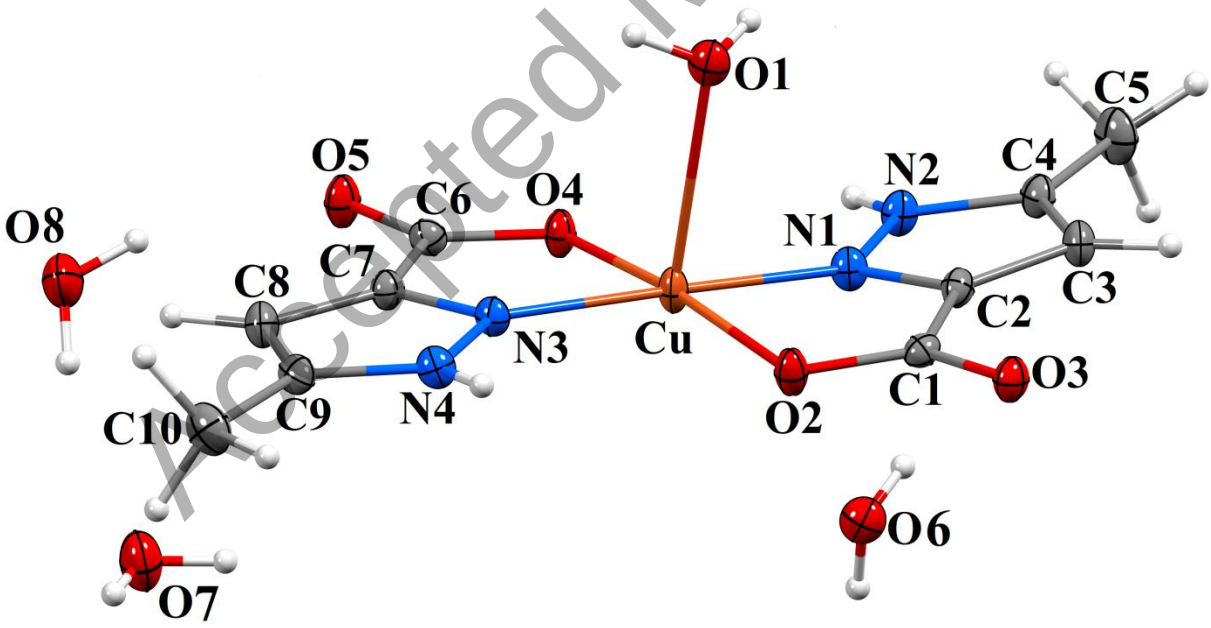

Figure 2. ORTEP of **1**.

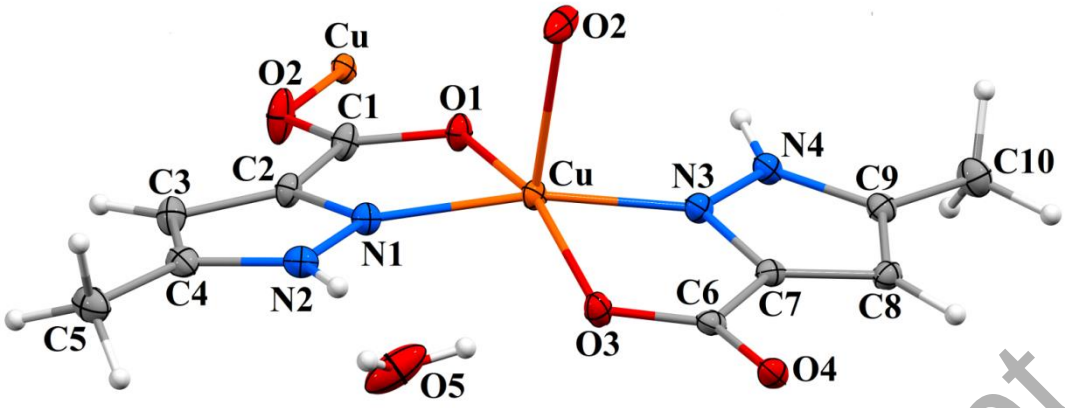

Figure 3. ORTEP of **2**. *Symmetry equivalent for O2i (i = x, 1/2-y, 1/2+z).

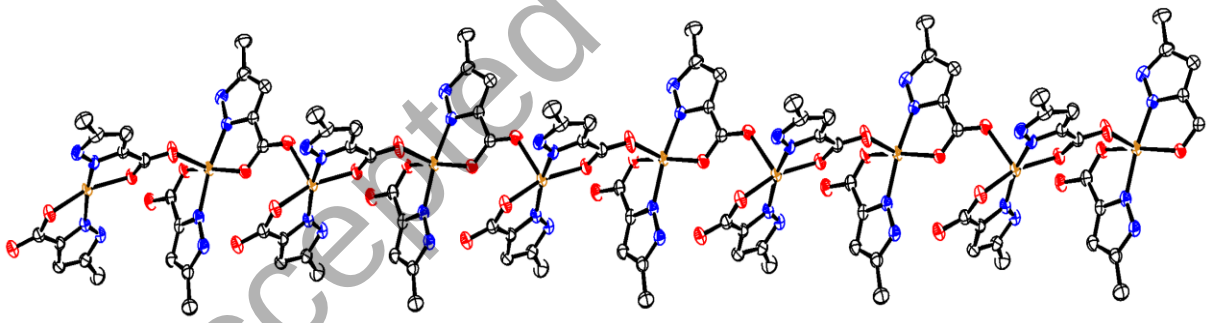

Figure 4. Polymeric structure of **2** viewed along the *b* axis (hydrogens are omitted for clarity).

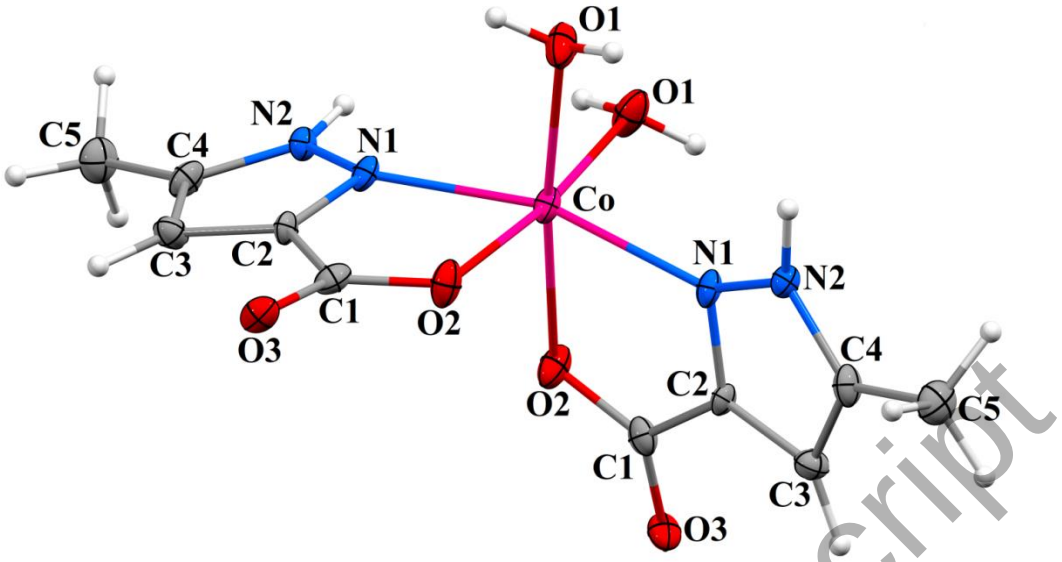

Figure 5. ORTEP of **3**.

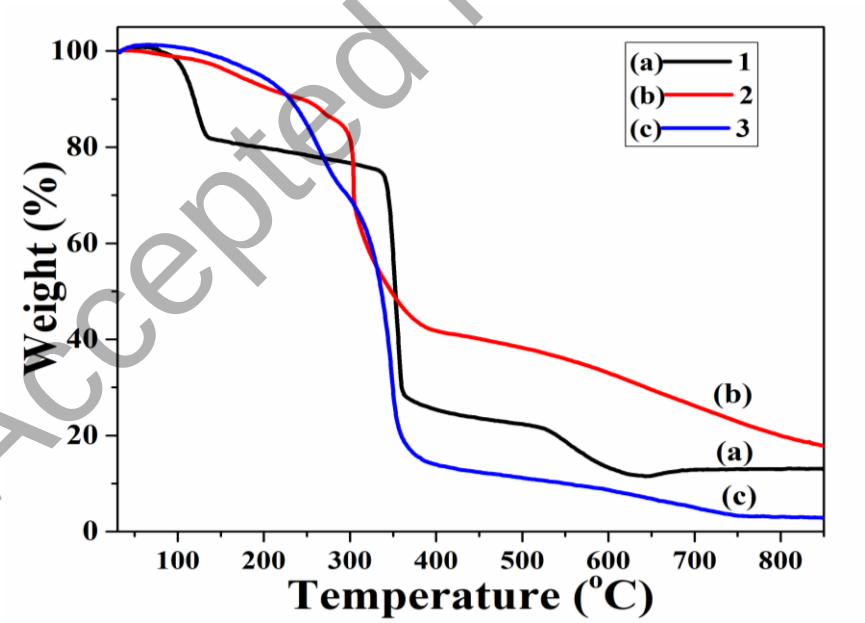

Figure 6. Thermogravimetric analysis of **1-3**.

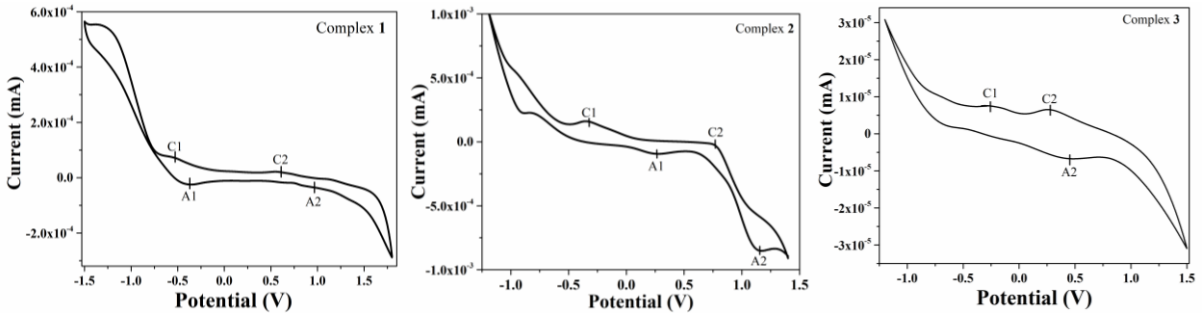

Figure 7. Cyclic voltammetry study of **1-3** in the presence of tertiary butyl ammonium perchlorate in methanol.

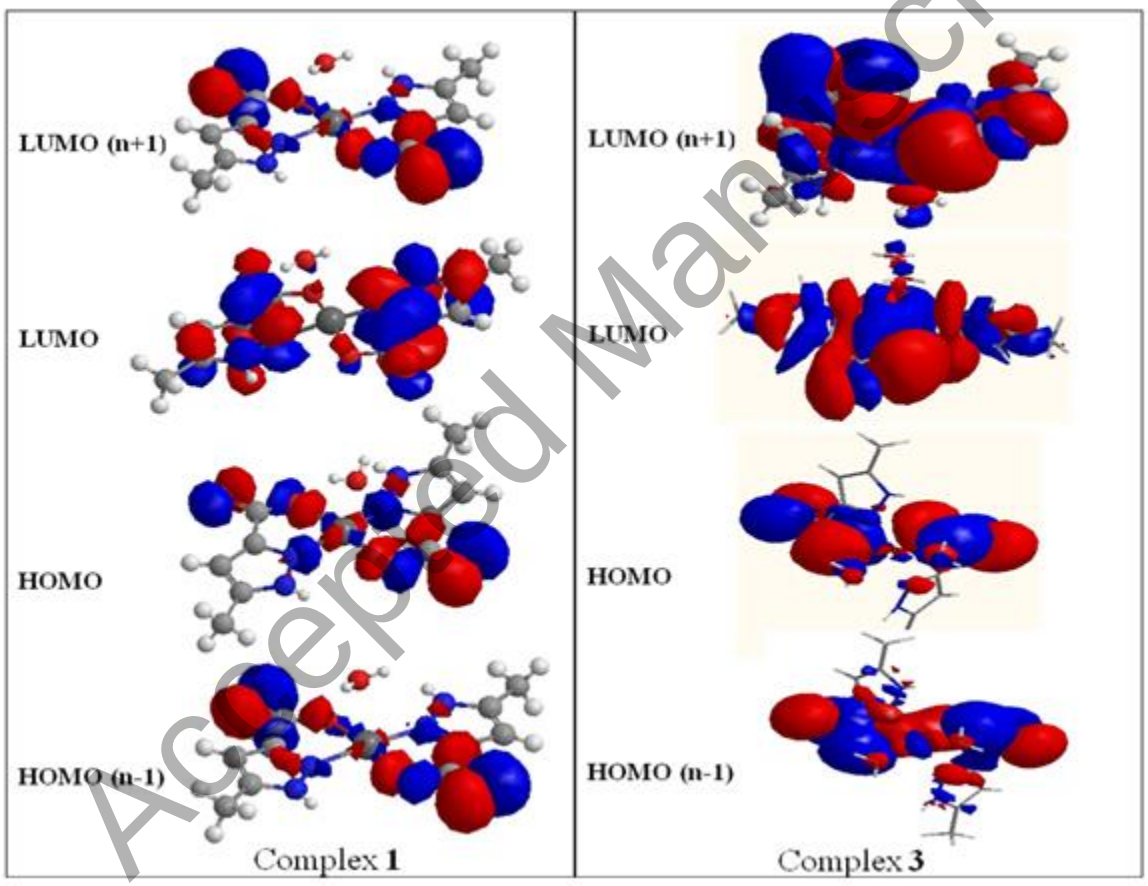

Figure 8. Surface plots of **1** and **3**.

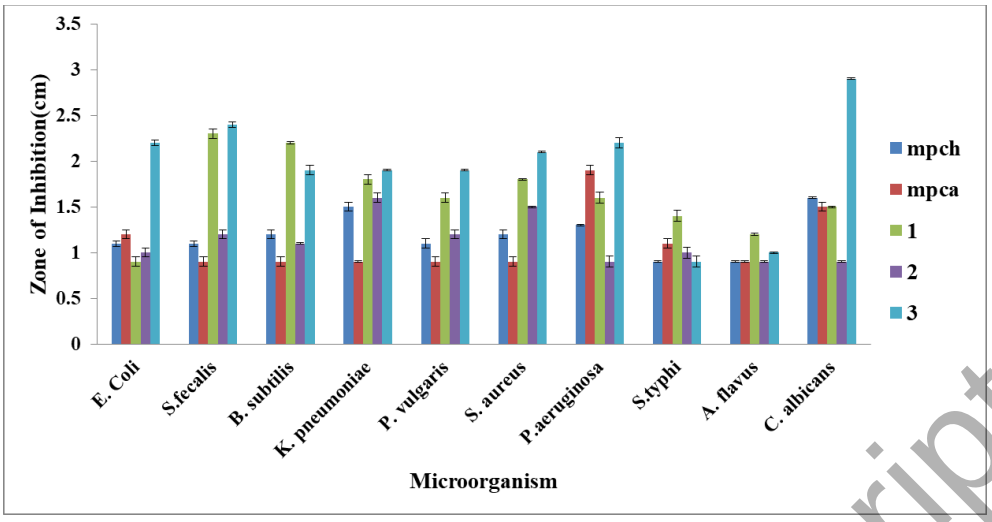

Figure 9. Graphical presentation of sensitivity of the compounds against different bacteria and fungi.

Table 1. Lipophilicity of the compounds determine by shake−flask method using UV-Vis spectroscopy.

Sample	1-Octanol		Water		log*P*
	Concentration (g/L)	Absorbance	Concentration (g/L)	Absorbance	
Hmpca	2.40	3.7923	1.39	2.116	0.2371
mpch	2.51	3.3218	1.68	2.2590	0.1743
1	2.07	3.2156	0.83	1.4972	0.3968
2	1.83	2.5292	1.45	2.014	0.1010
3	2.08	3.4714	0.47	0.7934	0.6459

Table 2. Crystal refinement parameters of **1**-**3**.

Parameters	**1**	**2**	**3**
CCDC	1826509	1826511	1826510
Mr	385.83	331.79	345.18
Moiety formula	$C_{10}H_{12}CuN_4O_5 \cdot 3(H_2O)$	$C_{10}H_{10}CuN_4O_4 \cdot H_2O$	$C_{10}H_{14}CoN_4O_6$
a (Å)	6.9787(6)	8.2401(2)	14.7463(13)
b (Å)	9.0648(7)	15.6756(5)	14.7463(13)
c (Å)	12.8706(10)	9.9014(3)	32.114(3)
α (°)	97.289(2)	90	90
β (°)	91.744(3)	104.88	90
γ (°)	112.178(2)	90	120
Crystal system	Triclinic	Monoclinic	Trigonal
Temperature	150K	150K	150 K
Volume	745.15(10)	1236.06(6)	6047.7(14)
Space group	*Pī*	*P 21/c*	*R −3 c*
μ (mm^{-1})	1.515	1.794	1.312
Z	2	4	18
F (000)	394.0	676.0	3150.0
F (000′)	394.84	677.55	3157.38
Dcalc (g cm^{-3})	1.711	1.783	1.686
R (reflections)	0.0337 (3269)	0.0279 (2835)	0.0964 (1337)
wR2 (reflections)	0.0858 (4037)	0.0705 (3348)	0.2252 (1499)

Table 3. Selected bond lengths (Å) of **1-3**.

1		**2**		**3**	
Atoms	Length (Å)	Atoms	Length (Å)	Atoms	Length (Å)
Cu−O1	2.466(2)	Cu−O1	1.988(1)	Co–O1	2.079
Cu−O2	1.963(1)	Cu−O3	1.987(1)	Co–O2	2.107
Cu−O4	1.963(1)	Cu−N1	1.955(2)	Co–N1	2.126
Cu−N1	1.941(2)	Cu−N3	1.970(2)	Co–O1	2.079
Cu−N3	1.954(1)	Cu−O2	2.209(2)	Co–O2	2.107
O2−C1	1.290(2)	O1−C1	1.278(2)	Co–N1	2.126
O3−C1	1.236(2)	O2−C1	1.245(3)	O2–C1	1.26(1)
O4−C6	1.291(3)	O2−Cu	2.209(2)	O3–C1	1.25(1)
O5−C6	1.234(2)	O3−C6	1.271(2)	N1–N2	1.346(8)
N1−N2	1.342(2)	O4−C6	1.252(2)	N1–C2	1.32(1)
N1−C2	1.340(3)	N1−N2	1.342(2)	N2–C4	1.34(1)
N2−C4	1.348(3)	N1−C2	1.336(3)	C1–C2	1.487(9)
N3−N4	1.343(2)	N3−N4	1.344(2)	C2–C3	1.41(1)
N3−C7	1.338(3)	N2−C4	1.354(3)	C3–C4	1.37(1)

Table 4. Selected bond angles (°) of **1**-**3**.

1		**2**		**3**	
Atoms	Angle (°)	Atoms	Angle (°)	Atoms	Angle (°)
O1–Cu–O2	88.28(6)	O1−Cu−O2	99.54(6)	O1–Co–O2	173.5
O1–Cu–O4	99.74(6)	O1−Cu−O3	160.53(5)	O1–Co–O1	88.1
O2–Cu–O4	171.62(6)	O3−Cu−O2	99.90(6)	O1–Co–O2	88.9
O1–Cu–N1	89.22(7)	O1−Cu−N1	81.55(6)	O1–Co–N1	96.7
O1–Cu–N3	93.30(6)	O3−Cu−N1	94.93(6)	O1–Co–N1	95.2
O2–Cu–N1	82.12(7)	O3−Cu−N3	81.91(6)	O2–Co–N1	77.7
O2–Cu–N3	99.73(6)	O1−Cu−N3	96.99(6)	O2–Co–O1	88.9
O4–Cu–N1	95.48(7)	N1−Cu−N3	166.36(6)	O2–Co–O2	94.6
O4–Cu–N3	82.33(6)	N1−Cu−O2	97.10(6)	O2–Co–N1	90.9
N1–Cu–N3	176.91(7)	N3−Cu−O2	96.51(6)	N1–Co–O1	95.2
Cu–O2–C1	114.3(1)	Cu−O1−C1	115.0(1)	N1–Co–O2	90.9
Cu–O4–C6	115.4(1)	C1−O2−Cu	126.4(1)	N1–Co–N1	163.3
Cu–N1–N2	139.1(1)	Cu−O3−C6	113.8(1)	O1–Co–O2	173.5
Cu–N1–C2	113.0(1)	Cu−N1−N2	139.4(1)	O1–Co–N1	96.7
N2–N1–C2	106.1(2)	Cu−N1−C2	114.1(1)	O2–Co–N1	77.7
N1–N2–H2	122(2)	N2−N1−C2	106.4(1)	Co–O2–C1	116.2
N1–N2–C4	111.7(2)	N1−N2−C4	111.1(2)	Co–N1–N2	139.5
H2–N2–C4	126(2)	H2−N2−C4	129(1)	Co–N1–C2	111.6
Cu–N3–N4	140.1(1)	Cu−N3−N4	140.9(1)	N2–N1–C2	105.9(7)
Cu–N3–C7	113.4(1)	Cu−N3−C7	112.9(1)	N1–N2–C4	111.6(7)
N4–N3–C7	106.1(2)	N4−N3−C7	106.1(1)	O2–C1–O3	124.2(8)

Table 5. Antimicrobial activity of specific concentration (1000 µg/mL) of different synthetic metal complex compared with control by agar well diffusion method.

Sample	Zone of inhibition (in cm) against (Mean±SD)									
	Bacteria								Fungi	
	Gram negative					Gram positive				
	E. coli	*S. typhi*	*B. subtilis*	*K. pneumoniae*	*P. vulgaris*	*S. aureus*	*P. aeruginosa*	S. *fecalis*	*A. flavus*	*C. albicans*
Hmpca	1.1 ±0.03	0.9 ±0.01	1.2 ±0.05	1.5 ±0.05	1.1± 0.05	1.2±0.05	1.3 ±0.01	1.1 ±0.03	0.9 ±0.01	1.6±0.01
mpch	1.2 ±0.05	1.1± 0.05	0.9 ±0.05	0.9 ±0.01	0.9± 0.05	0.9±0.05	1.9 ± 0.05	0.9 ±0.05	0.9 ±0.01	1.5±0.05
1	0.9 ±0.05	1.4 ±0.06	2.2 ±0.01	1.8 ±0.05	1.6±0.05	1.8±0.01	1.6 ±0.06	2.3 ±0.05	1.2 ±0.01	1.5 ±0.01
2	1.0 ±0.05	1.0 ±0.06	1.1 ±0.01	1.6 ±0.05	1.2±0.05	1.5±0.01	0.9 ±0.06	1.2 ±0.05	0.9 ±0.01	0.9 ±0.01
3	2.2 ±0.03	0.9 ±0.06	1.9 ±0.05	1.9 ±0.01	1.9±0.01	2.1±0.01	2.2 ±0.06	2.4 ±0.03	1.0 ±0.01	2.9±0.01
Flucanazole	-	-	-	-	-	-	-	-	1.1± 0.17	1.2±0.05
	Control									
MeOH	0.9±0.05	0.9±0.05	0.9±0.05	0.9±0.05	0.9±0.05	0.9±0.05	0.9±0.05	0.9±0.05	0.9±0.05	0.9±0.05

Table 6. MIC (minimum inhibitory concentration) value of different synthetic compound against bacteria and fungi.

Sample	MIC values (µg/ml) of samples									
	Bacteria								Fungi	
	Gram negative					Gram positive				
	E. coli	*S. typhi*	*B. subtilis*	*K. pneumoniae*	*P. vulgaris*	*S. aureus*	*P. aeruginosa*	*S. fecalis*	*A. flavus*	*C. albicans*
Hmpca	–	–	–	600	–	–	–	–	–	500
mpch	–	–	–	500	–	–	–	–	–	500
3	25	–	–	100	–	50	500	300	–	100
2	–	–	–	300	400	500	–	400	–	–
1	–	–	100	–	–	300	–	300	200	200

Graphical abstract